LA-UR- 01-2514 c.1

Approved for public release; distribution is unlimited.

Title: Equal Channel Angular Extrusion (ECAE) of Beryllium

Author(s): R.D. Field, MST-6
K. T. Hartwig, Texas A&M University
C. T. Necker, MST-6
J. F. Bingert, MST-6
S. R. Agnew, ORNL

Submitted to: Metallurgical and Materials Transactions A
(Proceedings of the "Defects, Properties and Mechanical Behavior of HCP Metals and Alloys" Symposium, TMS 2001 Annual Meeting)

Los Alamos
NATIONAL LABORATORY

Equal Channel Angular Extrusion of Beryllium

R.D. Field[†], K.T. Hartwig[††], C.T. Necker[†], J.F. Bingert[†], S.R. Agnew[†††]
[†] MST-6, Los Alamos Nationals Laboratory, Los Alamos, NM
[††] Mechanical Engineering Department, Texas A&M University, College Station, TX
[†††] Oak Ridge National Laboratory, Oak Ridge TN

Abstract

The Equal Channel Angular Extrusion (ECAE) technique has been applied to a P/M source Be alloy. Single and two-pass extrusions have been successfully completed, using two different processing routes, on Ni-canned billets of Be at 400°C. No cracking was observed in the billet and significant grain refinement was achieved. In this paper, microstructural features and dislocation structures are discussed for the single-pass material, including evidence of **<c>** and **<c+a>** dislocations. Significant crystallographic texture developed during ECAE, which will be discussed in terms of this unique deformation processing technique and the underlying physical processes which sustained the deformation.

Introduction

Equal channel angular extrusion (ECAE) is a method for introducing large amounts of simple shear deformation in a material and effecting a high degree of microstructural refinement (i.e grain and/or subgrain size). The reader is referred to comprehensive reviews for details of the process and deformation modes [1, 2]. Most ECAE studies have been performed on cubic materials in which a sufficient number of independent slip systems are available to produce homogeneous plasticity. Hexagonal close packed (hcp) materials exhibit highly anisotropic plastic properties at the grain level. The implications of this fact on the deformation and texture development during ECAE processing of an hcp metal (Mg) has been investigated previously by one of us [3].

In the current investigation, Be billets were subjected to both single and two-pass ECAE processing. Microstructural characterization of the billets was performed using both optical and TEM techniques to investigate grain refinement and deformation microstructures. In addition, texture development was characterized by x-ray and electron backscatter diffraction (EBSD) techniques. The experimental results are compared to results from deformation modeling using a viscoplastic self-consistent (VPSC) code. In this paper, results from the single pass billet will be presented. Results from the 2-pass billets will be presented in a subsequent publication.

Experimental Procedure

The starting material for this study was P/M source Be, designated as P31664, which was produced by the Brush-Wellman company by vacuum hot pressing of attrited powder. Cylinders of this material 0.75" diameter by 5.5" long (19.1mm x 139.7mm) were removed from the bulk using wire electro-discharge machining (EDM) and machined to fit 1" square by 6" long (25.4mm x 152.4mm) Ni 200 cans. The Be pieces were vacuum annealed for one hour at 800°C to relieve machining stresses before being placed in the cans. A plug with a step joint was then electron beam welded onto the top of the can.

Figure 1 is a schematic of the ECAE extrusion process. The reader is referred to the previously listed references for a detailed description [1,2]. Three billets were extruded: a

single pass, two passes with no rotation (Route A), and two passes with a 180° rotation (Route C). The extrusions were performed in a warm tool (350°C) through a sharp 90° angle at a nominal billet temperature of 425°C and with a punch velocity of 25.4 mm/s, which corresponds to a strain rate of approximately 10 s^{-1}. The combined effects of rapid deformation, thermal isolation of the Be by the Ni can and a lower temperature tool are estimated to have led to a temperature rise of the Be to perhaps 475°C during extrusion. The maximum adiabatic temperature rise is calculated to be 490°C. The extrusion events were unremarkable and exhibited expected load-stroke behavior. The peak loads seen for the first and second extrusion passes were nominally 250,000 and 350,000 lbs. force (1.11×10^6 and 1.56×10^6N), respectively.

Following extrusion, the billets were sliced along the flow plane (see Figure 1), using wire EDM. One half of the billet was metallographically prepared to reveal overall macro- and microstructure of the extrusion. Additional pieces were sectioned from the other half for heat treatments, transverse metallographic specimens, transmission electron microscopy (TEM), and texture measurements. No signs of cracking were observed in any of the sections. Some pieces were subjected to 1 hour heat treatments at 600, 700, and 800°C to study recrystallization and grain growth of the extruded material. These specimens were encapsulated in quartz tubes, which were evacuated, flushed and backfilled with Ar and sealed. The heat treatments were conducted in a resistance tube furnace.

Metallographic preparation was performed using standard techniques. TEM foils were made by first taking 350-500μm slices using a diamond saw in the flow plane. The slices were then ground to ~150μm using 400-600 grit SiC paper and 3mm discs removed using an abrasive core drill. The foils were thinned to perforation in a Fischione automatic electropolishing unit, using a solution of 8% perchloric acid, 20% water, 12% isobutyl alcohol, and 60% methanol at a temperature of -50°C and a potential of 65V. Transmission electron microscopy was performed in a Philips CM30 instrument at an accelerating potential of 300KV.

Bulk x-ray diffraction (XRD) texture measurements were collected on metallographic samples using reflection geometry on a Huber four-circle goniometer and Scintag x-ray machine with Fe Kα radiation. The (0001), $(10\bar{1}0)$, and $(10\bar{1}1)$ pole figures were collected and used to determine the orientation distribution function (ODF) by use of the WIMV algorithm within the popLA software package [4]. The ODF was then used to recalculate full pole figures. Spatially resolved microtexture scans were performed on colloidal silica-polished sections using automated electron back-scattered diffraction (EBSD) in a Philips XL30 FEG SEM, while TSL's OIM software was used for analysis.

Deformation Modeling

The viscoplastic self-consistent (VPSC) code [5] was used to simulate the texture evolution during ECAE. The VPSC approach explicitly incorporates the anisotropic interactions between individual grains and the surrounding polycrystalline aggregate. This is done in order to realistically distribute the strain between the grains, while insuring the overall imposed strain is accommodated by the aggregate. The importance of this capability for the current application is twofold. First, Be displays significant plastic anisotropy at the grain level (see Table 1). Second, grain shapes become very anisotropic during the ECAE process, which will also influence the strain distribution.

Table I. Deformation modes and CRSS values for 99.9% Be at 400°C (derived from **[6]**)

Deformation Mode	Crystallography	CRSS (MPa)	Relative CRSS
Basal <a> Slip	$<11\bar{2}0>\{0001\}$	5	1
Prism <a> Slip	$<11\bar{2}0>\{10\bar{1}0\}$	10	2
Pyramidal <c+a> Slip	$<11\bar{2}3>\{11\bar{2}2\}$	150	30
Tensile Twinning	$<10\bar{1}0>\{10\bar{1}2\}$	40	8

For simulations of deformation textures, a straining path must be specified. This is done in the form of a velocity gradient tensor, **L**.

$$\mathbf{L} = \mathbf{D} + \mathbf{W};$$

where **D** is the symmetric rate-of-deformation tensor, and **W** is the antisymmetric spin tensor. For many common deformation processes such as axisymmetric tension (extrusion or drawing) or compression (upset forging) or pure shear (plane strain compression or rolling) there is no macroscopically imposed spin. However, the ECAE process imposes a *simple shear* strain upon the workpiece. In such cases the spin is a critical part of the imposed velocity gradient. The reader is referred to the discussions of Kocks [7] and Bolmaro and Kocks [8] for more complete treatments of the relative importance of spin in different deformation processes.

The simulations were performed using a computer generated random texture represented by 1000 discrete orientations. A c/a ratio of 1.5677 was assumed and the deformation modes and associated critical resolved shear stresses (CRSS) used for these simulations are given in Table 1. A stress exponent of 20 was used in the viscoplastic constitutive equation for all the deformation modes and no attempt was made to include the effect of slip system hardening or latent hardening. The tangent formulation of VPSC was employed. Since no twinning was observed in the simulations, this subject will not be discussed here. The reader is referred to an earlier paper by Tomé, Lebensohn, and Kocks [9] for a discussion of the twinning model used in VPSC.

Results

In Figure 2, optical and TEM micrographs of the starting material are shown. This material has a nominal grain size of 11μm; however, Figure 2 reveals a wide range of grain diameters. X-ray texture measurement of this material showed it to have a nearly random texture (maximum of 1.4x random). Figure 3 shows flow and transverse plane optical micrographs. The flow plane section (Figure 3a) contains elongated grains with diagonal shear bands, while the transverse plane section reveals a horizontal, flattened grain structure (Figure 3b). This is consistent with previous investigations of ECAE microstructures after a single pass [10]. Heat treatments of 500, 600, 700, and 800°C for 1 hour were conducted. Evidence of recrystallization was observed for the 700 and 800°C heat treatments, in the form of more equiaxed grain structure. However, very little grain growth was observed up to 700°C, and some grain refinement was still retained after the 800°C heat treatment. Vickers hardness measurements (Figure 4) show decreasing strength for heat treatments at 600°C and above, with the hardness returning to approximately that of the as-received material after the 800°C treatment.

The low magnification TEM micrograph of Figure 5 shows the elongated grain structure in the flow plane cross-section. Several dislocation networks, representing the development of low angle boundaries (LAB's) are visible in the micrograph (note, in particular, the lower right corner of the micrograph), lying across the elongated grains. Similar structures, consisting of elongated grains crossed by LAB's, have been noted previously in Cu processed by ECAE [11]. One of these features is shown in more detail in Figure 6. This LAB consists of $\mathbf{b}=1/3[\bar{2}110]$ dislocations in near edge orientation. Thus, the LAB is primarily a tilt boundary in this instance. The angular mismatch can be estimated from the dislocation spacing to be approximately 0.7°. Several examples can be seen in which matrix dislocations are incorporated into the network.

Another LAB is shown in Figure 7. As in the previous case, instances of matrix dislocations entering the LAB are clearly visible. The dislocations in this boundary are in-contrast for a (0002) **g**-vector indicating a **<c>** component to their Burgers vector. A complete Burgers vector analysis was conducted on these dislocations. They were found to be invisible for $(\bar{1}010)$ and $(0\bar{1}10)$ **g**-vectors, indicating a Burgers vector of $\mathbf{b}=[0001]$. Results from trace analyses of the segments in the matrix and in the LAB revealed line directions close to $[11\bar{2}0]$ and [0001], respectively. Thus, the dislocations are in the edge orientation in the matrix and the screw orientation within the LAB. Thus, the LAB is a twist boundary. As before, an estimate of the angular mismatch can be made from the dislocation spacing, which was calculated to be approximately 0.6°, comparable to the $\mathbf{b}=1/3[\bar{2}110]$ tilt boundary analyzed above.

Dislocations with [0001] Burgers vectors have been associated with both the decomposition of **<c+a>** dislocations [12, 13] and debris from $\{10\bar{2}2\}$ deformation twinning [14] in hcp materials. In order to distinguish between these two sources, evidence for both **<c+a>** slip and deformation twinning was sought. While no indications of the latter were found, **<c+a>** dislocations were observed, as shown in Figure 8. Along with LAB's consisting of normal **<a>** dislocations (bottom of micrographs), two sets of **<c+a>** dislocations are observed in this grain. That these are **<c+a>** dislocations is demonstrated by the fact that they are in contrast for both the (0002) and $(\bar{1}010)$ **g**-vectors. A complete Burgers vector analysis was conducted, in which the out of contrast conditions were recorded for both $(10\bar{1}\bar{1})$ and $(01\bar{1}\bar{1})$ **g**-vectors, yielding of Burgers vector of $\mathbf{b}=1/3[11\bar{2}3]$. The two sets of dislocations have the same Burgers vector, but different line directions; neither line direction is consistent with a $\{11\bar{2}2\}$ slip plane, however. Thus, these dislocations appear to have undergone some climb recovery.

Results from the EBSD experiments are presented in Figures 9 and 10. Figure 9a is a grain direction map of a flow plane cross-section, referenced to a color-keyed inverse pole figure for hexagonal crystals. The solid lines indicate boundaries with angular misorientation values in excess of 15°. It can be seen from the figure that the grain refinement associated with the ECAE processing is largely in the form of high-angle boundaries (i.e. >15°). A considerable number of sub-boundaries, depicted by hue variations in Figure 9a, are also present, consistent with TEM observations. These boundaries result in an accumulation of misorientation, as shown in the two orientation traces shown in Figures 9b and 9c. Individual sub-boundaries ("point-to-point" data) of <1° to ~10° result in accumulated misorientations of up to 30° over 10-20μm distances ("point-to-origin" data).

In addition to the general boundary analyses described above, the specific orientation relationships associated with the $\{10\bar{1}2\}$ twinning system were sought from the EBSD data, with a tolerance of ±5°. As in the TEM investigations, no evidence of this twinning system was found. In Figure 10, pole figures generated from the EBSD data are presented. These are comparable to the XRD pole figures shown in Figure 11, showing the relative scale independence of the texture.

A comparison between pole figures generated from XRD texture data and calculated texture profiles from the VPSC code are presented in Figure 11. Although the severity of the texture is overpredicted by the simulation, the general features of the experimental texture are reproduced in the calculated data. For both experiment and simulation, the maximum intensity of the basal pole peaks correspond to basal planes inclined with the elongated grains. Figure 12 shows the relative contributions of the different slip systems to deformation in the VPSC simulation. Note that no twinning and negligible <**c+a**> slip is activated in the simulation, suggesting <**a**> slip is able to accommodate the simple shear deformation.

Discussion

Experiments conducted thus far have been preliminary in nature, with only single and double ECAE passes. However, the results are encouraging, indicating that significant grain refinement of Be is possible using the ECAE technique, without cracking of the material. This grain refinement can be maintained after thermal exposures of 1 hour at temperatures up to at least 700°C. The EBSD data have shown much of this grain refinement to be in the form of high angle boundaries.

Both TEM and EBSD data indicate that deformation during extrusion is effected by slip mechanisms, with little or no contribution from twinning. The extremely low ratio of the critical resolved shear stresses for basal and prismatic slip compared to that of any other deformation systems in Be, even at elevated temperatures, means that <**a**> dislocations dominate the structure. However, a significant number of <**c**> dislocations, as well as some <**c+a**> dislocations, are present. In the absence of any evidence for twinning, the <**c**> Burgers vector is believed to be debris from the decomposition of <**c+a**> dislocations. It is interesting to note, however, that the presence of LAB's consisting of **b**=[0001] dislocations indicates that this species has at least some limited mobility in the material. It should be noted that slip of <**c**> dislocations cannot be activated during uniaxial straining without incurring a substantial resolved shear stress on the highly favored basal <**a**> systems. Thus, the simple shear nature of deformation during the ECAE process may represent a unique opportunity for <**c**> dislocations to contribute to plasticity. The significant hydrostatic stresses (on the order of the flow stress of the material) which develop during the extrusion may also affect the activation of slip systems. However, it should also be noted that the VPSC code was able to simulate the experimental texture without significant contributions from non-<**a**> slip systems. It is likely, therefore, that the role of <**c**> and <**c+a**> dislocations is primarily to alleviate local incompatibilities between grains and that these Burgers vectors only make a minor contribution to overall plasticity.

Conclusions

Preliminary experiments on the application of the ECAE technique to Be have demonstrated the potential for significant grain refinement without cracking. Investigation of deformation mechanisms via texture simulation using a viscoplastic self-consistent approach indicate the majority of plasticity is effected by basal slip, with significant contributions from prismatic slip. Transmission electron microscopic investigation has suggested that local incompatibilities are alleviated by the motion of <**c+a**> dislocations. Evidence for at least limited mobility of <**c**> dislocations has also been found, since they are observed to organize into low angle boundaries. VPSC modeling of deformation associated with ECAE has successfully reproduced the salient features of texture development, although the intensity

of the texture is overpredicted. A similar analysis of the two pass billets has been conducted and will be presented in a subsequent publication.

Acknowledgements

The authors would like to thank Pallas Papin for her assistance in preparing and performing preliminary examinations of TEM foils, and Dr. Robert Hanrahan for performing the post-ECAE heat treatments, as well as technical discussions. Technical discussions with Dr. Dan Thoma and Steve Abeln also contributed significantly to this work. Work at LANL was supported under U.S. DOE Contract No. W-7405-ENG-36. SRA would like to acknowledge support for this work from the U.S. DOE, Assistant Secretary for Energy Efficiency and Renewable Energy, Office of Transportation Technologies, as part of the Office of Heavy Vehicle Technologies Program, under contract DE-AC05-00OR22725 with ORNL, operated by UT/Battelle, LLC for DOE.

References

1. V.M. Segal: Mater. Sci. Eng., 1995, vol. A197, pp. 157-164.
2. V.M. Segal, R.E. Goforth, and K. T. Hartwig: Apparatus and Method for Deformation Processing of Metals, Ceramics, Plastics, and Other Materials, 1995, United States Patent No. 5,400,633.
3. S.R. Agnew, T.M. Lillo, J. Macheret, G.M. Stoica, L. Chen, Y. Lu, D. Fielden, and P.K. Liaw: in Magnesium Technology 2001, J. Hryn, ed., 2001, TMS, Warrendale, PA. pp. 243-248.
4. J.S. Kallend, U.F. Kocks, A.D. Rollett, and H.-R. Wenk: Mater. Sci. Eng., 1991, vol. A132, pp. 1-11.
5. R.A. Lebensohn and C.N. Tomé: Acta Metall. Mater., 1993, vol. 41, pp. 2611-2624.
6. D. Webster, G.J. London, D.R. Floyd, and J.N. Love: Beryllium Science and Technology, Plenum Press, New York, 1979.
7. U.F. Kocks: in Texture and Anisotropy, U.F. Kocks, C.N. Tomé, and H.-R. Wenk, eds., 1998, Cambridge University, New York.
8. R.F. Bolmaro and U.F. Kocks: Scripta Metall. Mater., 1992, vol. 27, pp. 1717-1722.
9. C.N. Tomé, R.A. Lebensohn, and U.F. Kocks: Acta Metall. Mater., 1991, vol. 39, pp. 2667-2680.
10. S. Ferasse, V.M. Segal, K.T. Hartwig, and R. Goforth: Metall. Mater. Trans., 1997, vol. 28A, pp. 1047-1057.
11. S.R. Agnew, U.F. Kocks, K.T. Hartwig, and J.R. Weertman: in 19th Risø Int. Symp. on Mat. Sci., Roskilde, Denmark, 1998, pp. 201-206.
12. J.P. Poirier, J. Antolin, and H.M. Dupouy: Can. J. Phys., 1967, vol. 45, pp. 1221-1224.
13. V.V. Damiano, G.L. London, and H. Conrad: Trans. Metall. Soc. AIME, 1968, vol. 242, pp. 987-994.
14. S. Morozumi, M. Kikuchi, and H. Yoshinaga: Trans. JIM, 1976, vol. 17, pp. 158-164.

a)

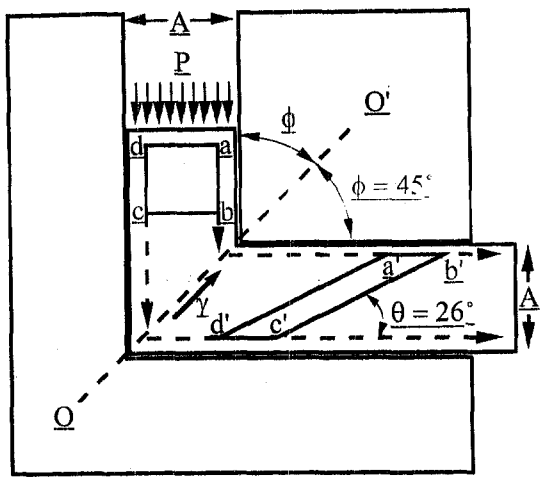

b)

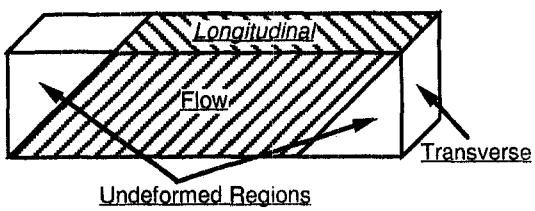

Figure 1. Schematics showing the ECAE process. a) The billet is extruded through an angled die ($2\phi = 90°$ in the current study), causing the original cube element abcd to deform by simple shear to the parallelpiped a'b'c'd', and resulting in a Von Mises equivalent strain of 1.15. Since the cross-sectional areas before and after extrusion (A) are equivalent, the billet can be subjected to multiple passes through the same die. b) Depiction of the extruded billet showing deformed and undeformed regions, and the definitions of principal billet planes.

Figure 2. Microstructure of the starting Be material (prior to ECAE processing), a) light optical micrograph, b) TEM micrograph.

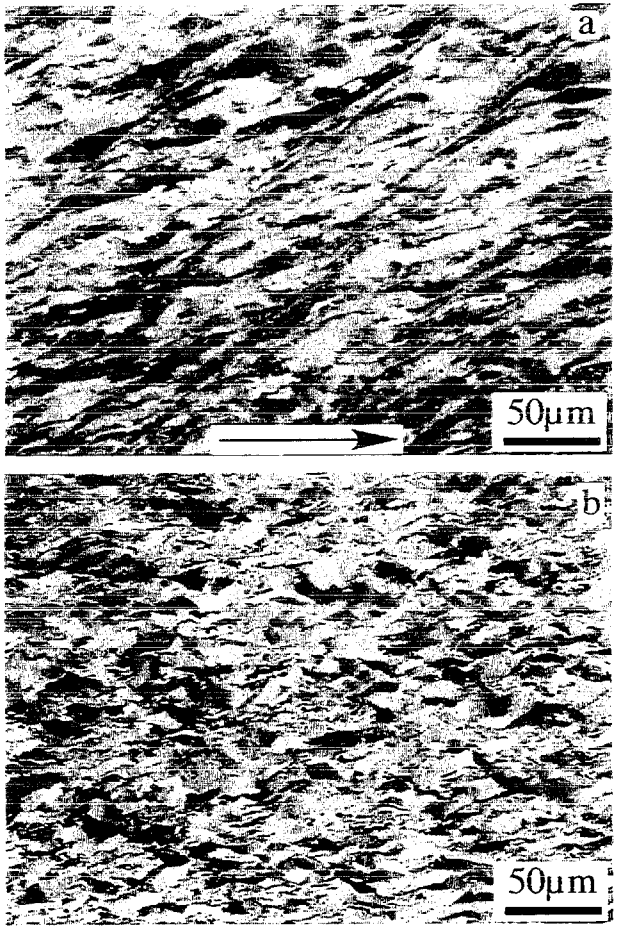

Figure 3. Light optical micrographs of the as-extruded (single pass) ECAE material, a) flow plane cross-section (arrow indicates extrusion direction), b) transverse cross-section.

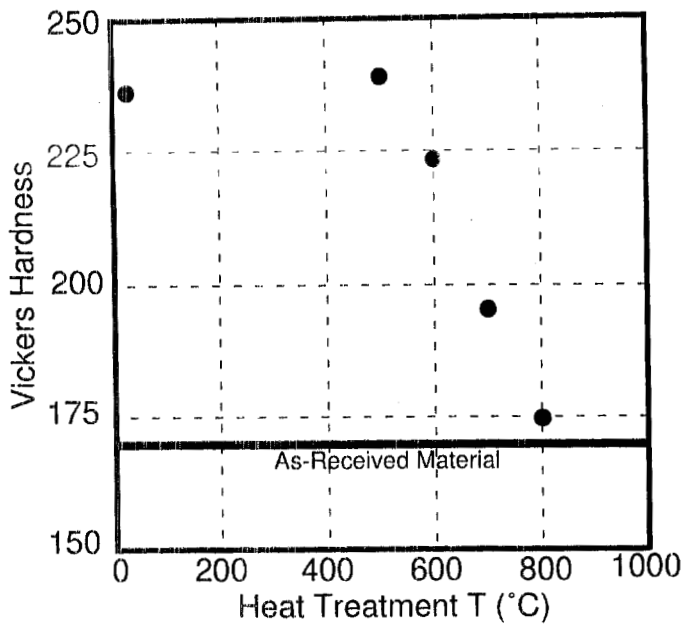

Figure 4. Plot of Vickers hardness values as a function of post ECAE annealing temperature (1 hour anneals). The horizontal line marks the hardness value of the starting material. The value at 23°C is for the as-extruded specimen.

Figure 5. TEM micrograph of the as-extruded specimen flow plane cross-section, arrow indicates extrusion direction.

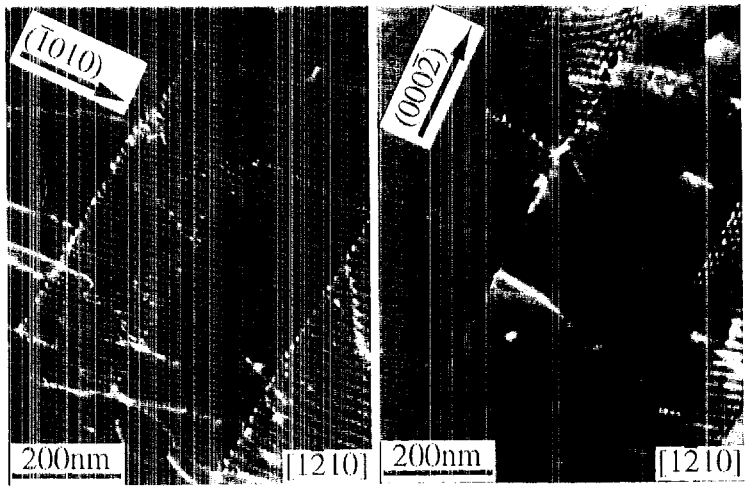

Figure 6. Weak beam TEM micrographs of a low angle boundary in the as-extruded specimen, consisting of $\mathbf{b}=1/3[\bar{2}110]$ dislocations.

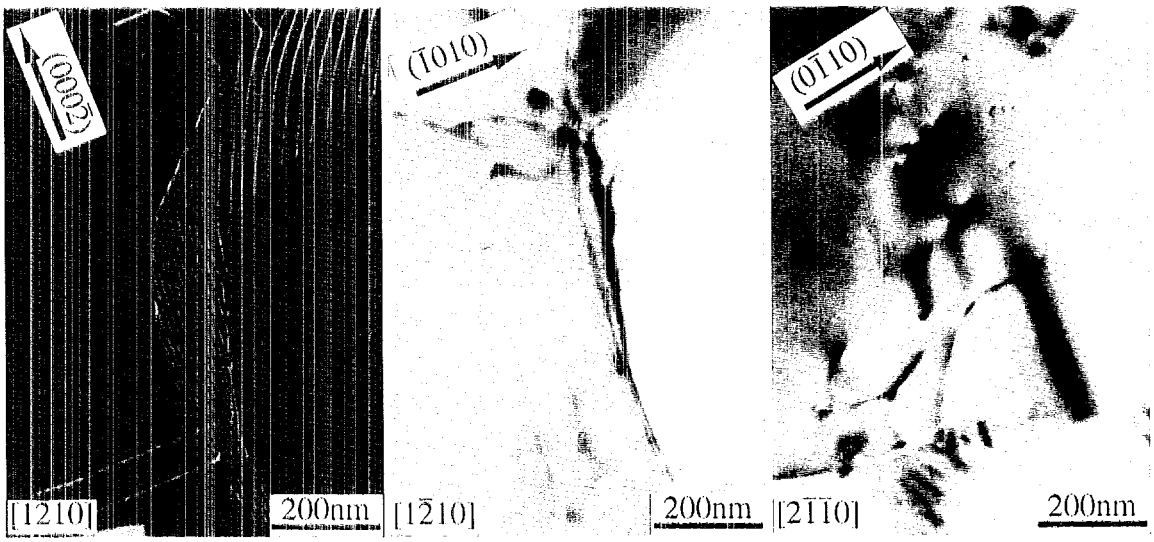

Figure 7. TEM micrographs of a low angle boundary in the as-extruded specimen, consisting of **b**=[0001] dislocations, a) weak beam micrograph showing dislocations in contrast for **g**=(0002), b) and c) bright field micrographs showing the dislocations out of contrast for **g**=($\bar{1}$010) and **g**=(0$\bar{1}$10).

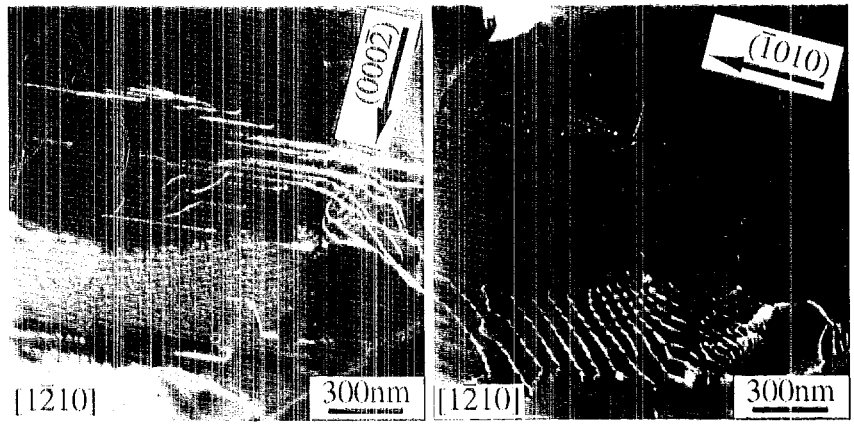

Figure 8. Weak beam TEM micrographs of **b**=1/3[11$\bar{2}$3] dislocations in the as-extruded specimen. That these are "**c+a**" dislocations is demonstrated by the fact that they are in contrast for both the (0002) and ($\bar{1}$010) **g**-vectors.

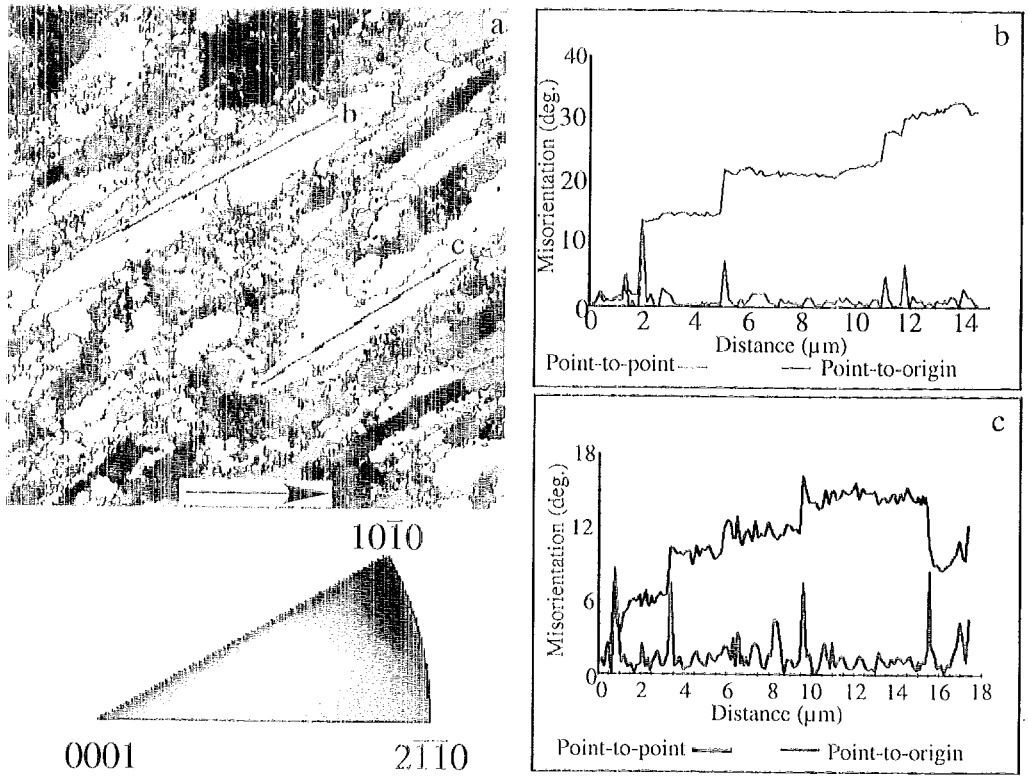

Figure 9. Results from EBSD experiments on ECAE material: a) grain direction map (flow plane cross-section) and orientation key (step size = 150nm, boundaries with misorientations >15° are outlined in black, arrow indicates extrusion direction). b and c) plots of accumulated misorientation along lines drawn on (a).

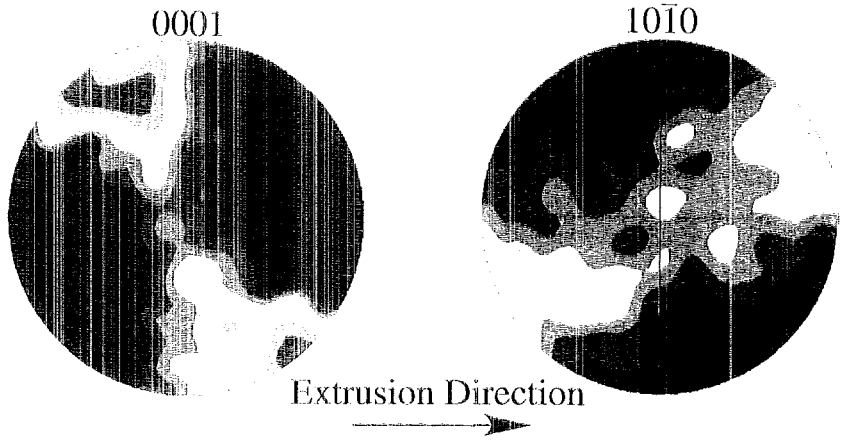

Figure 10. Pole figures derived from EBSD experiments of ECAE material (flow plane cross-section). These compare favorably with the x-ray data in Figure 11.

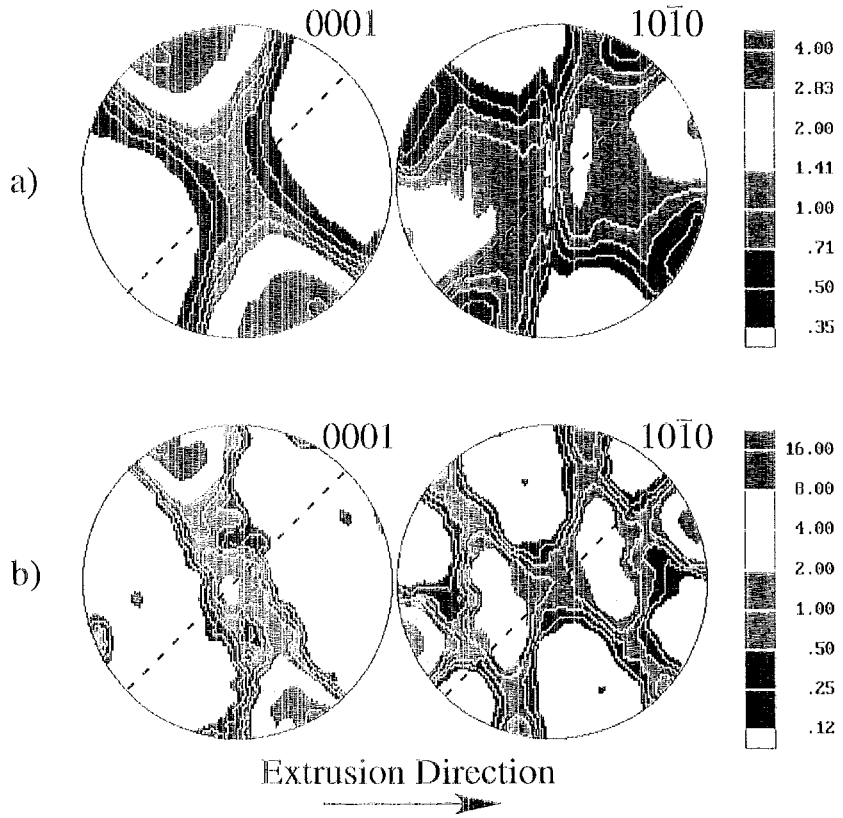

Figure 11. Comparison between experimental x-ray texture data (recalculated from ODF) (a) and VPSC simulated texture (b) after one pass ECAE. The simple shear plane is indicated by the dashed line. The pole figures are equal area projections, where the discrete textures generated by the simulation code were smoothed over 5° for comparison with experimental data collected on a 5° grid. (flow plane cross-section)

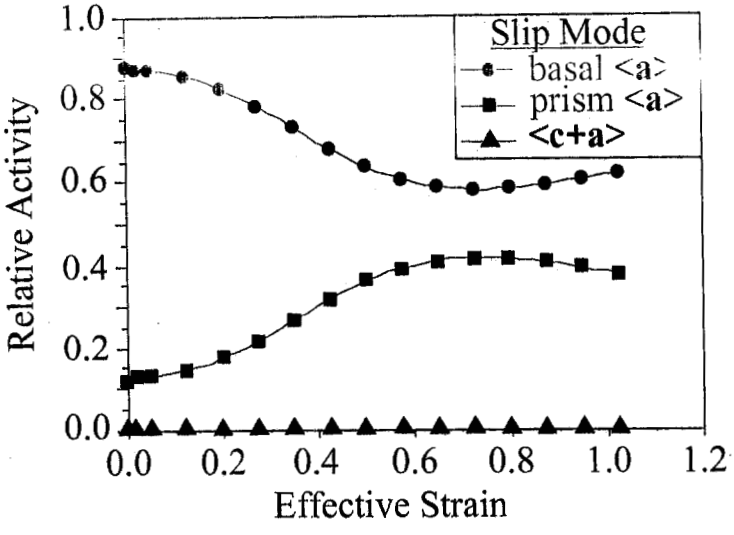

Figure 12. Relative contributions of the different slip systems to deformation in the VPSC simulation. Note that no twinning and negligible **<c+a>** slip is activated in the simulation.